

Analyst

Accepted Manuscript



This is an *Accepted Manuscript*, which has been through the Royal Society of Chemistry peer review process and has been accepted for publication.

Accepted Manuscripts are published online shortly after acceptance, before technical editing, formatting and proof reading. Using this free service, authors can make their results available to the community, in citable form, before we publish the edited article. We will replace this *Accepted Manuscript* with the edited and formatted *Advance Article* as soon as it is available.

You can find more information about *Accepted Manuscripts* in the [Information for Authors](#).

Please note that technical editing may introduce minor changes to the text and/or graphics, which may alter content. The journal's standard [Terms & Conditions](#) and the [Ethical guidelines](#) still apply. In no event shall the Royal Society of Chemistry be held responsible for any errors or omissions in this *Accepted Manuscript* or any consequences arising from the use of any information it contains.

Facile Synthesis of Boron and Nitride Doped MoS₂ nanosheets as Fluorescence Probes for Ultrafast, Sensitive, and Label-free Detection of Hg²⁺

Xiaojia Liu, Liping Li, Yuanjie Wei, Yizhi Zheng, Qian Xiao, Bo Feng*

College of Chemical Engineering, Xiangtan University, Xiangtan 411105, Hunan Province, China

Abstract: Bulk MoS₂, a prototypical transition metal chalcogenide material, is an indirect band gap semiconductor with negligible photoluminescence. In this study, we develop, for the first time, a simple and low-cost synthetic strategy to prepare boron, nitrogen-doping MoS₂ (B,N-MoS₂) nanosheets. Through boron and nitrogen doping, the band gap of MoS₂ increases from 1.20 eV to 1.61 eV, and the obtained B,N-MoS₂ nanosheets exhibit enhanced fluorescence. The B,N-MoS₂ nanosheets can be used as a green and facile sensing platform for label-free detection of Hg²⁺ because of its high sensitivity and selectivity toward Hg²⁺. In addition, detection can be easily accomplished through one-step rapid (within 2 min) operation, with a limit as low as 1 nM. This study demonstrates the introduction of boron and nitrogen elements into ultrathin MoS₂ nanosheets for enhanced fluorescence properties is feasible through a facile and general preparation strategy, and may also offer a unique idea as a potential way to design more efficient MoS₂-based sensors and fluorescence materials.

Keyword: B,N-MoS₂; fluorescence; sensor; Hg ion; mechanism

1. Introduction

Mercury ion has been recognized as one of the most toxic transition metal ion in the world by the United States Environment Protection Agency (USEPA)^{1,2}. Even at low concentration, mercury ion is a huge threat to humans and the environment because of its ability of accumulate in the ecological system³. Mercury poisoning induces a wide variety of serious human diseases, such as brain damage, kidney failure, and cognition and motion disorders^{4,5}. Therefore, facile, rapid, and sensitive methods for efficient detection of Hg²⁺ ions are highly

1
2
3 desirable. Traditional techniques for Hg^{2+} analysis, include cold vapor atomic fluorescence
4 spectroscopy, atomic absorption spectroscopy, and inductively coupled plasma mass
5 spectrometry⁶⁻⁸, which are very sensitive and accurate. However, these methods involve
6 sophisticated instruments, time-consuming complicated synthetic processes, and large amount
7 of sample^{9,10}, among others. To overcome these disadvantages, fluorescence sensors have
8 recently received significant attention because of their simple operation, high sensitivity,
9 low-cost, and efficiency¹¹.

10
11
12 Since the discovery and wide investigation of graphene, a great deal of attention has been
13 given to two-dimensional layered materials¹²⁻¹⁴ because of their fascinating optical, electronic,
14 mechanical, and electrochemical properties¹⁵⁻¹⁸. The ability to prepare graphene offers new
15 possibilities and research into the chemistry and physics of two-dimensional layered
16 material¹⁹⁻²³. Transition metal dichalcogenides, such as MoS_2 , are one of the most important
17 graphene analogues. MoS_2 is a quasi-two-dimensional compound, with covalently bonded
18 S–metal–S sheets held by van der Waals forces, such as that in graphene²⁴. MoS_2 nanosheet has
19 attracted significant attention because of its excellent energy conversion, piezoelectronics,
20 nanoelectronics, and optoelectronics properties³⁹. With its unique properties, MoS_2 has been
21 applied in various fields, including energy conversion²⁵, hydrogen evolution catalysis²⁶⁻²⁸,
22 Li-ion batteries²⁹⁻³¹, cell-targeted labeling²⁴, fluorescence materials^{32,33} and biosensors^{34,35}.

23
24
25 The absence of a band gap in graphene leads to very low $I_{\text{on/off}}$ ratio, thereby limiting its
26 broader use for applications in electronics such as logic devices³⁶. Compared with graphene,
27 MoS_2 with band gaps around 1.2 eV to 1.9 eV has attracted increasing attention in recent years
28 and has shown wide application potential in optoelectronics^{37,38}. Inspired by the great advances
29 in graphene research, researchers have develop several methods^{39,40} to control band gap of the
30 MoS_2 . Bulk MoS_2 has a band gap around 1.2 eV; monolayer MoS_2 has a band gap around 1.8
31 eV; and single-layer MoS_2 has a band gap around 1.9 eV. Ultrathin, ultrasmall, defect, and
32
33
34
35
36
37
38
39
40
41
42
43
44
45
46
47
48
49
50
51
52
53
54
55
56
57
58
59
60

1
2
3 doped⁴¹⁻⁴³ MoS₂ prepared by different researchers to control their band gaps have shown
4
5 excellent applications in semiconductors and fluorescence materials.
6

7
8 In this study, using the doping method to change the band gap of MoS₂, we report, for the
9
10 first time, a facile and low-cost synthetic strategy to prepare fluorescent nanosheets of
11
12 B,N-MoS₂ by doping MoS₂ with boron and nitride. The B,N-MoS₂ nanosheets can serve as a
13
14 highly effective fluorescent probe for sensitive detection of Hg²⁺, with a detection limit of as
15
16 low as 1 nM in 2 min, which is much lower than that the previously reported fluorosensors.
17
18 This sensor is also applied successfully for Hg²⁺ determination in tap water sample, with a
19
20 detection limit of 100 nM. The proposed design is simple to prepare and exhibits low
21
22 background interference, high sensitivity, and ultrafast response.
23
24

25 **2. Experimental section**

26 2.1 Materials

27
28 CaCl₂, CoCl₂, Fe(NO₃)₃, Hg(Ac)₂, Mn(NO₃)₂, Pb(NO₃)₂, Zn(Ac)₂, Ni(NO₃)₂, NaNO₃, KNO₃,
29
30 Cd(NO₃)₂, Ba(NO₃)₂, Mg(NO₃)₂, Cu(NO₃)₂, LiNO₃, and AgNO₃ were purchased from Aladin
31
32 Ltd. (Shanghai, China). All chemicals were used as received without further purification. All
33
34 solutions employed throughout the experiments were prepared using deionized Milli-Q water.
35
36

37 2.2 Characterizations

38
39 The morphology of the products was investigated by scanning electron microscopy (SEM)
40
41 (Hitachi S-4800, Japan) at 5.0 kV accelerating voltage. X-ray diffraction (XRD) analysis was
42
43 carried out on a BRUKER D8-ADVANCE X-ray diffractometer using Cu (40 kV, 40 mA)
44
45 radiation. Raman spectra were obtained using a laser confocal Raman spectrometer
46
47 (LABRAM-010) in the range of 300 cm⁻¹ to 2000 cm⁻¹. Transmission electron microscopy
48
49 (TEM) images were obtained with JEM-3010 (JEOL-3010, Japan). The atomic force
50
51 microscopy (AFM) (Bioscope system, Bruker, USA) study was performed using a tapping
52
53 model. Metrology X-ray photoelectron spectroscopy (XPS) was carried out using K-Alpha
54
55
56
57
58
59
60

1
2
3 1063 type with focused monochromatized Al K α radiation (1486.6 eV). Fluorescent emission
4
5 spectra were recorded on a F-7000 spectrofluorometer (Hitachi, Japan). Ultraviolet–visible
6
7 (UV–vis) spectra were recorded with a UV-1800 spectrophotometer (Shimadzu, Japan).
8
9

10 2.3 Synthesis of B₃N-MoS₂

11 In a typical synthesis, the bulk MoS₂ (0.5 g) was thoroughly mixed with a solution of boric
12 acid (2 g) and melamine (2 g) in anhydrous ethanol (100 mL) by ultrasonic dispersion for 1 h.
13
14 The mixture was dried at 80 °C and then heated to 400 °C in N₂ atmosphere at a heating rate of
15
16 5 °C min⁻¹ and maintained for 2 h. The sample was cooled to room temperature to obtain the
17
18 B₃N-MoS₂ powder. In a typical run, 10 mg of B₃N-MoS₂ powder was added to 100 mL of
19
20 deionized water. After ultrasonic dispersion for 2 h, the precipitate was removed by
21
22 centrifugation at 2000 rpm for 3 min, and the clear supernatant extract was prepared for
23
24 analysis.
25
26
27
28

29 2.4 Detection of Hg ions

30
31 Detection of Hg ions was performed at room temperature in aqueous solution. Hg aqueous
32 solutions with different concentrations, together with other metal ion solutions, were freshly
33 prepared before use. To evaluate the sensitivity towards Hg²⁺, different concentrations of Hg²⁺
34 were added into the aqueous solutions containing the same amount of B₃N-MoS₂; the mixed
35 solutions were equilibrated for 2 min before spectral measurements. The photoluminescence
36 (PL) spectra were recorded by operating the fluorescence spectrophotometer at 280 nm
37 excitation wavelength.
38
39
40
41
42
43
44
45
46

47 3. Results and discussion

48 3.1 Characterizations of B₃N-MoS₂

49
50 The SEM image of bulk MoS₂ shown in Fig. 1 (a) indicates that they are solid agglomerates
51 approximately several micrometers in size and exhibit the accumulation of large structures.
52
53 B₃N-MoS₂ presents a thin layer structure as shown in Fig. 1 (b), demonstrating that boron and
54
55
56
57
58
59
60

1
2
3 nitrogen-doped MoS₂ two-dimensional layered ultrathin nanosheets were prepared after doping
4
5 and ultrasonication.
6

7
8 In addition, the crystalline structure of bulk MoS₂ and B,N-MoS₂ were determined by
9
10 powder XRD [Fig. 1 (c)]. The peaks at 14.4°, 32.8°, 39.6°, 49.8°, and 58.5° correspond to the
11
12 (002), (100), (103), (105), and (110) reflections of bulk MoS₂ (indexed by JCPDS no. 37-1492),
13
14 respectively. For B,N-MoS₂, the peaks at 14.3°, 32.6°, 39.5°, 49.8°, and 58.4° correspond to
15
16 the (002), (100), (103), (105), and (110) reflections, respectively. Compared with bulk MoS₂,
17
18 the d-spacing of B,N-MoS₂ increases from 0.6133 nm to 0.6186 nm, indicating that B and N
19
20 were doped into the MoS₂ structure.
21

22
23 The difference between the in-plane (E_{2g}^1) and out-of-plane (A_{1g}) Raman modes (Δk) is an
24
25 appropriate quantity to assign the number of MoS₂ layers on various substrates^{12,19}. Figure 1 (d)
26
27 shows the Raman spectra of bulk MoS₂ and B,N-MoS₂ measured at 632 nm excitation laser
28
29 line. For the bulk sample, the two Raman characteristic bands at 402 and 373 cm⁻¹ that
30
31 correspond to the A_{1g} and E_{2g}^1 vibration modes show a peak frequency difference of 29 cm⁻¹,
32
33 namely, $\Delta k=29$ cm⁻¹. However, for B,N-MoS₂, the two Raman characteristic bands at 402 and
34
35 379 cm⁻¹ corresponding to the A_{1g} and E_{2g}^1 vibration modes show a peak frequency difference
36
37 of 23 cm⁻¹, namely, $\Delta k=23$ cm⁻¹. This result agrees well with the results of other researchers
38
39 ^{12,19,33,38}, indicating that the B,N-MoS₂ comprises 6 layers of MoS₂, as confirmed by the AFM
40
41 test [3.9 nm, nearly 6 layers, Fig. 2 (c) and (d)].
42
43
44
45
46
47
48
49
50
51
52
53
54
55
56
57
58
59
60

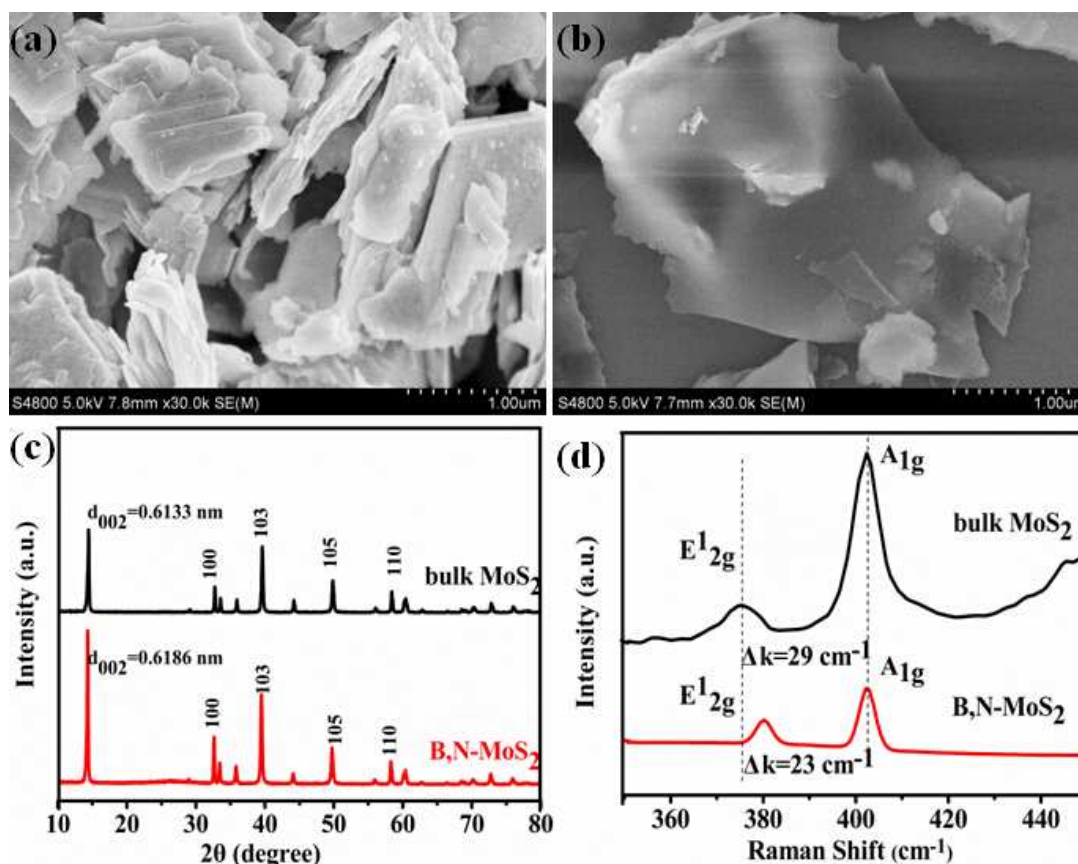


Fig. 1 SEM images of bulk MoS₂ (a) and B,N-MoS₂ (b); XRD pattern of bulk MoS₂ and B,N-MoS₂ (c); Raman spectra of bulk MoS₂ and B,N-MoS₂ (d).

TEM and AFM were carried out to further analyze the layer structure of B,N-MoS₂. The morphologies of the as-prepared B,N-MoS₂ were characterized by TEM. Fig. 2 (a) shows the image of B,N-MoS₂, wherein three layers of B,N-MoS₂ overlapped together. The edge of the overlap image can be seen clearly in Fig. 2 (b). Fig. 2 (a) and (b) indicate that the layered nanosheets were successfully prepared. The inset of Fig. 2 (b) shows the high resolution transmission electron microscopy (HRTEM) image of B,N-MoS₂, with the (002) crystal plane spacing of 0.62 nm of the lattice. The result fits well with the XRD result. The energy spectrum (EDS) (Supporting Information, Fig. S1) further implied that boron and nitrogen elements were successfully doped into MoS₂ nanosheets.

The AFM test shown in Fig. 2 (c) (d) indicates that B,N-MoS₂ nanosheets consist of few

layer MoS₂; this result agrees well with SEM, TEM, and Raman analysis (shown in Fig. 1). The thickness test [Fig. 2 (d)] showed that the concrete thickness of B,N-MoS₂ is 3.9 nm, and the two-dimensional layer number is approximately 6 layers (the thickness of the single-layer MoS₂ is approximately 0.62 nm).

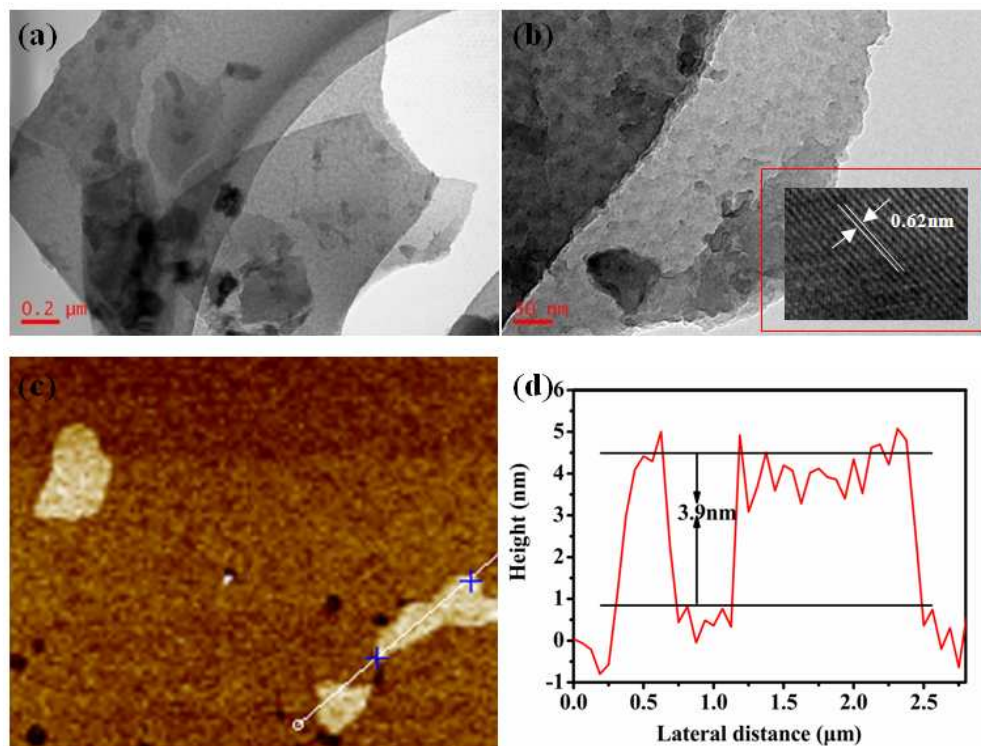


Fig. 2 TEM (a), HRTEM (b), AFM (c), and Height analysis (d) of B,N-MoS₂.

XPS was conducted to analyze the chemical states of Mo and S in the bulk MoS₂ and B,N-MoS₂ samples (Fig. 3). According to the full survey spectra [Fig. 3 (a)], the elements Mo, S, C, and O are found on all the samples; however, B and N are found on the B,N-MoS₂ sample, indicating that B and N were successfully doped into MoS₂. The Mo 3d XPS spectrum of the bulk MoS₂ sample [Fig. 3 (b)] shows two broad peaks at 228.9 and 232.0 eV, which can be indexed as the doublet Mo 3d_{5/2} and Mo 3d_{3/2}, respectively. A small S 2s peak is located at 226 eV. The XPS spectrum of B,N-MoS₂ shows three peaks at 226.1, 229.1, and 232.1 eV, similar to the bulk MoS₂ sample. The peaks at 161.5 and 162.9 eV, corresponding to the S 2p_{3/2} and S 2p_{1/2} of divalent sulfide ions (S²⁻), are shown in Fig. 3 (c). These binding energies are in

good agreement with the reported values for the MoS₂ samples^{43,44}. However, the peaks corresponding to the S 2p_{3/2} and S 2p_{1/2} shifted toward higher binding energies (161.9 eV, 163.3 eV), indicating that boron and nitrogen elements were successfully doped into MoS₂. These results agree with the EDS result of the B,N-MoS₂ sample (Supporting Information, Fig. S1).

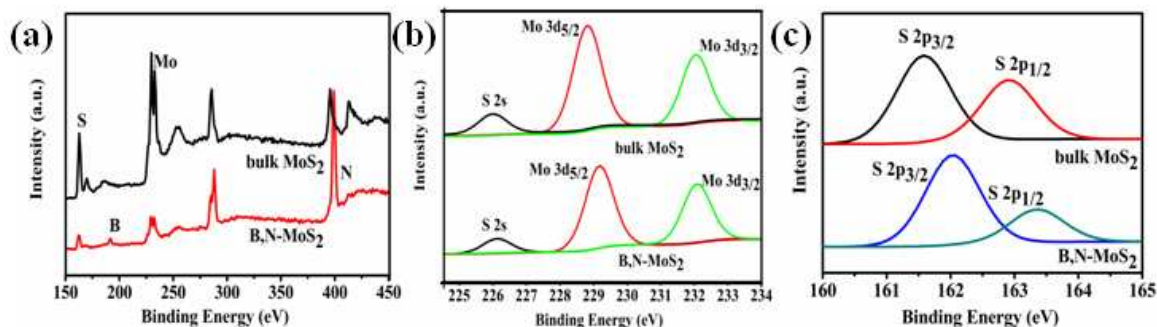


Fig. 3 XPS spectra of B,N-MoS₂.

Fig. 4 shows the photoluminescent (PL) emission spectra of B,N-MoS₂, bulk MoS₂ and few-layer MoS₂ at a same concentration, with excitation at 280 nm. Notably, the fluorescence of the bulk MoS₂ and few-layer MoS₂ dispersion can almost be ignored. However, the dispersion of B,N-MoS₂ showed a strong PL emission peak centered at 343 nm, indicating that the nanosheets are fluorescent.

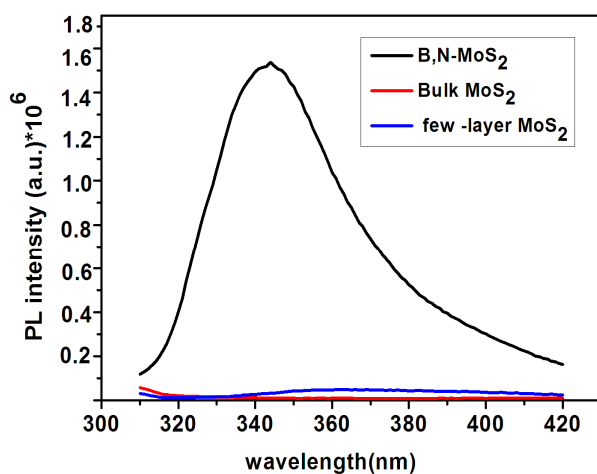


Fig. 4 PL spectra of B,N-MoS₂, bulk MoS₂ and few-layer MoS₂ ($\lambda_{ex} = 280$ nm).

3.2 Novel fluorescence property of B,N-MoS₂.

Fig. 5 (a) shows the UV-vis absorption and PL emission spectra of B,N-MoS₂ dispersion in water. The UV-vis spectrum shows an absorption peak at 250 nm. The dispersion exhibits a strong PL emission peak centered at 343 nm when excited at 280 nm, indicating that the B,N-MoS₂ nanosheet has strong fluorescence. Fig. 5 (b) shows the emission spectra of B,N-MoS₂ at different excitation wavelengths; the emission spectra are not dependent on the excitation wavelength. This finding is different from the PL spectra of large scale single-layer MoS₂ nanosheets; that is, B,N-MoS₂ does not have any emission peaks from 450 nm to 600 nm^{45,46}. However, these spectra are similar to the emission spectra of MoS₂ quantum dots⁴⁷, which have blue photoluminescence at 415 nm at different excitation wavelengths from 270 nm to 350 nm, indicating that B,N-MoS₂ has a novel fluorescence property different from layer MoS₂ and MoS₂ quantum dots.

Fig. 5 (c) shows the PL quenching results of B,N-MoS₂ in the presence of Ca²⁺, Co²⁺, Fe³⁺, Hg²⁺, Mn²⁺, Pb²⁺, Zn²⁺, Ni²⁺, Na⁺, K⁺, Cd²⁺, Ba²⁺, Mg²⁺, Cu²⁺, Li⁺ and Ag⁺ (50 μM). As shown in Fig. 5 (c), obvious PL quenching was observed upon the addition of Hg²⁺. Among the tested ions, only Fe³⁺ at high concentration may interfere with Hg²⁺ detection. Fortunately, this issue can be circumvented using triethanolamine (TEA) as chelating agents of Fe³⁺ ions, as shown in Supporting Information (Fig. S2). The addition of Fe³⁺ into the B,N-MoS₂-Hg²⁺ mixture in the presence of chelating agents has no effect on the detection of Hg²⁺. These observations indicate that other metal ions slightly influence the Hg²⁺ sensing system.

Aside from selectivity, sensitivity is another important parameter in evaluating the performance of a sensing system. Therefore, the PL intensity changes with time were studied to evaluate the sensitivity of the sensing system in this study. As shown in Fig. 5 (d), the time-dependent plot indicates that only 2 min is required to complete the reaction between B,N-MoS₂ and Hg²⁺. Therefore, the detection is ultrafast.

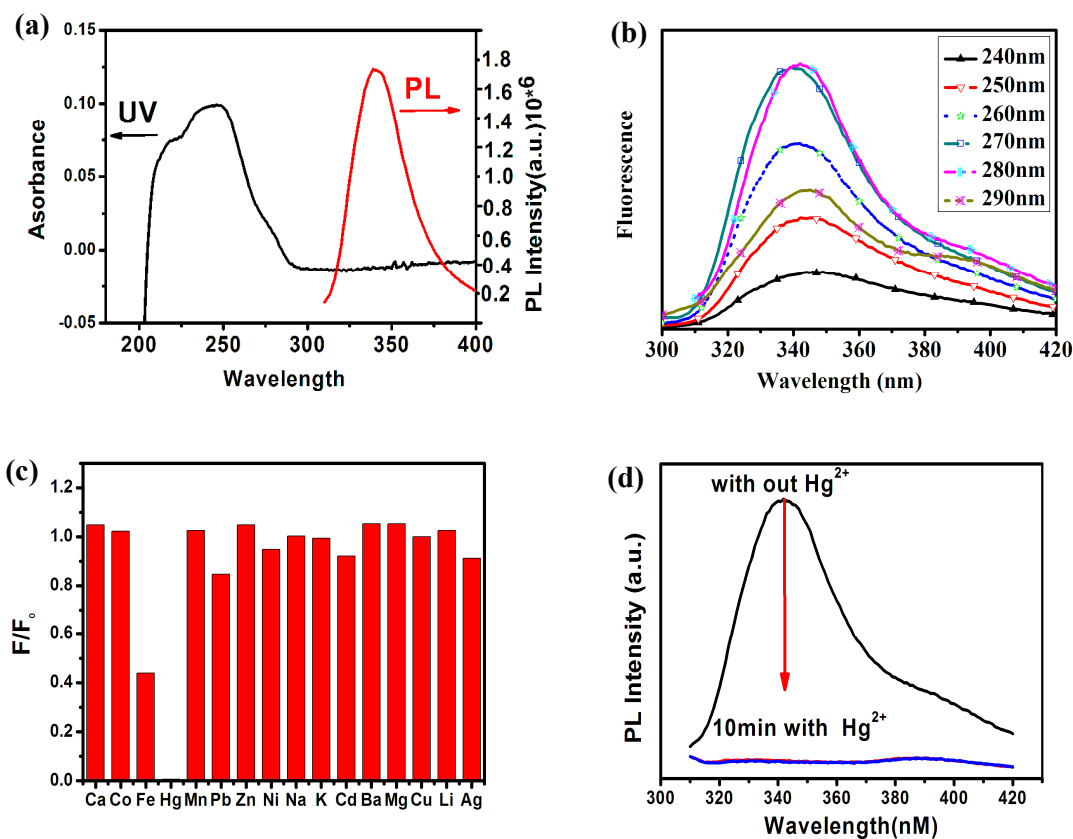


Fig. 5 UV and PL spectra of B,N-MoS₂ (a); PL spectra of B,N-MoS₂ at different excitation wavelengths (b); Selective PL response of aqueous B,N-MoS₂ solution towards different metal ions ($\lambda_{\text{ex}} = 280$ nm, F_0 and F are the fluorescence intensities of B,N-MoS₂ at 343 nm in the absence and presence of metal ions) (c); Time-dependent PL spectra of B,N-MoS₂ dispersion after the addition of 5 μM Hg²⁺ ($\lambda_{\text{ex}} = 280$ nm) (d).

Fig. 6 (a) shows the PL spectra of the B,N-MoS₂ solution with different concentrations of Hg²⁺. The result indicates that the PL intensity of the mixture is sensitive to Hg²⁺ concentration and decreases with the increase in Hg²⁺ concentration. Fig. 6 (b) shows the dependence of F/F_0 on Hg²⁺ concentration, where F_0 and F represent the fluorescence intensities of B,N-MoS₂ at 343 nm in the absence and presence of Hg²⁺, respectively. A good linear correlation was obtained over the concentration range of 0.01 μM to 3.0 μM ($R=0.9904$). The detection limit was estimated to be 1 nM at a signal-to-noise ratio of 3 (From top to bottom: 0, 0.00125,

0.0025, 0.005, 0.01, 0.0125, 0.25, 0.5, 1.0, 2.0, 2.5, and 3.0 μM of Hg^{2+}). As shown in Fig. 6 (c) and (d), our sensor was also applied successfully for Hg^{2+} determination in tap water sample, with a detection limit of 100 nM. The proposed design is simple to prepare and exhibits low background interference, high sensitivity, and ultrafast response.

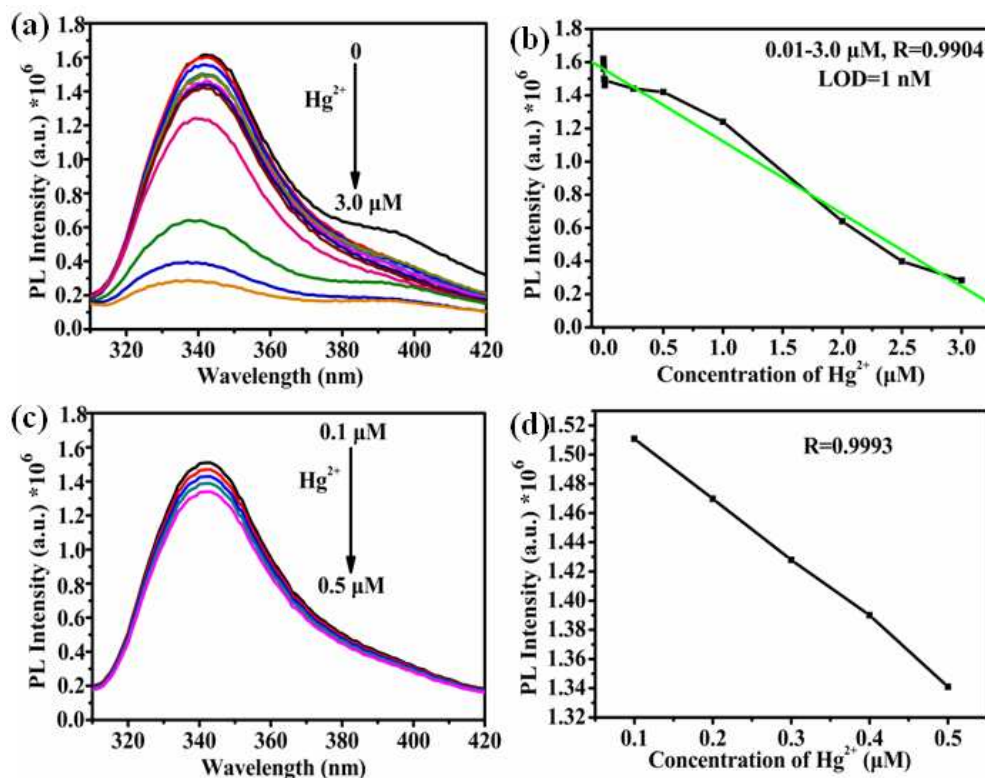


Fig. 6 PL spectra of B,N-MoS₂ at different Hg^{2+} concentrations (a); Linear relation of fluorescent probes for Hg^{2+} (b); Fluorescent probes for Hg^{2+} in tap water (c) (d).

Table 1 compares the sensing performance of different fluorescent probes for Hg^{2+} , showing that our sensing system exhibits superior sensitivity over previously reported sensing systems.

Table 1 Comparison of different fluorescent probes for Hg^{2+} detection.

Materials	Linear range	Detection limit	Reference
CdSe/ZnS quantum dots	---	10 nM	48
Carbon nanodots	0–3.0 μM	4.2 nM	49

Au cluster–CdTe quantum dots	0.131–0.71 μM	9 nM	50
ssDNA-GO	0.03–0.18 μM	30 nM	51
Gold nanoparticle	0.025–4.0 μM	10 nM	52
squaraine dye	1.0–10.0 μM	13 nM	53
graphene oxide/Ru-complex	0–6.0 μM	2.34 nM	54
mesoporous cerium phosphonate	0.05–1.5 μM	16 nM	55
carbon dots and graphene oxide	0.005–0.2 μM	2.4 nM	56
carbon nanoparticles	0.5–10 μM	10 nM	57
B,N-MoS ₂	0.01–3.0 μM	1.0 nM	This work

3.3 Fluorescence quenching mechanism, band gap analysis of B,N-MoS₂

As shown in Fig. 7, we used the doping method to change the band gap of MoS₂. The solid UV tests show that bulk MoS₂ has a band gap around 1.20 eV, which agrees well with the results of several researchers⁴¹⁻⁴⁴. However, the band gap of B,N-MoS₂ is very interesting, which is around 1.61 eV. Six layers of MoS₂ obtain a band gap around 1.4 eV⁵⁸. After doping, the band gap of B,N-MoS₂ increased from 1.2 eV to 1.61 eV. XPS is a common characterization method to analyze the valence band of semiconductors⁵⁹; we used this tool to analyze the valence band of bulk MoS₂ and B,N-MoS₂. The valence band of bulk MoS₂ and B,N-MoS₂ are 0.4 eV apart (Supporting Information, Fig. S3). This result agrees well with the UV test result. Therefore, this doping method significantly changed the band gap of MoS₂ successfully.

The introduction of Hg²⁺ into dispersion leads to significant decrease in fluorescence intensity, indicating that Hg²⁺ can effectively quench the fluorescence of B,N-MoS₂ nanosheets. The chelation of Hg²⁺ with sulfur elements of the B,N-MoS₂ nanosheets brings them into close proximity with each other. Given that the redox potential of Hg²⁺/Hg⁺ lies between the

conduction band (CB) and valence band (VB) of B,N-MoS₂, photoinduced electron transfer (PET) from the CB to the complex Hg²⁺ occurs, leading to fluorescence quenching (Fig. 7 a).

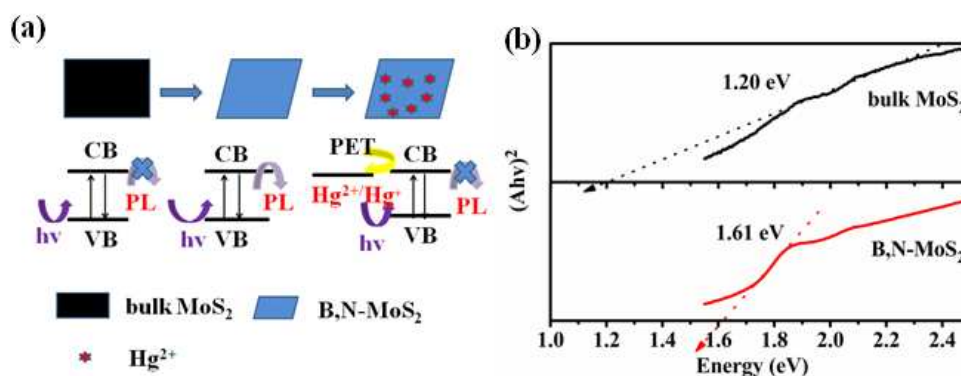


Fig. 7 Scheme of sensing principle of the B,N-MoS₂ nanosheet based fluorescence sensor for Hg²⁺ (a); Band gaps of MoS₂ and B,N-MoS₂ (b).

4. Conclusions

In summary, we developed a simple method for the preparation of B,N-doped MoS₂ with boric acid and melamine as boron and nitrogen sources, respectively. The as-synthesized B,N-MoS₂ exhibited enhanced fluorescence compared with the undoped MoS₂ and utilized as a highly efficient fluorescence sensor for selective detection of Hg²⁺ for the first time. The detection is rapid, taking only 2 min, and ultrasensitive, with a very low detection limit of 1 nM. We also demonstrated its application for tap water sample analysis. The present study provided a simple, low-cost route toward production of B,N-MoS₂ for sensing, bioimaging, optical imaging, and other applications. This novel strategy may inspire the exploration of an economic, stable, and environment-friendly fluorescent probes for rapid, highly selective, and sensitive optical detection of Hg²⁺. This work successfully demonstrated that the introduction of boron and nitrogen elements into ultrathin MoS₂ nanosheets for enhanced fluorescence properties is feasible through a facile and general preparation strategy. This method may open up a potential way for designing more efficient MoS₂-based biosensors and fluorescence material.

5. Acknowledgements

This work was supported by National Natural Science Foundation of China (31270988), Undergraduate Innovational Experimentation Program of Xiangtan University (2014xtuxj40), Scientific Research Fund of Hunan Provincial Education Department (13B120), China Postdoctoral Science Foundation (2014M562118) and Hunan Provincial Natural Science Foundation of China (2015JJ2133).

References

- (1) A. Shin, K. Kazunori, *J. Am. Chem. Soc.*, 2011, 133, 2556.
- (2) Environmental Standards for Mercury, Background Information on Mercury Sources and Regulations, United State Environmental Protection Agency (EPA)., www.epa.gov.
- (3) A. Bernaus, X. Gaona, J. M. Esbrí, P. Higuera, G. Falkenberg, M. Valiente, *Environ. Sci. Technol.*, 2006, 40, 4090.
- (4) J. Lee, H. Jun, J. Kim, *Adv. Mater.*, 2009, 21, 3674.
- (5) S. Liu, X. Y. Qina, J. Q. Tian, L. Wang, X. P. Sun, *Sens. Actuators B Chem.*, 2012, 171, 886.
- (6) F. Y. Chen, S. J. Jiang, *J. Agric. Food Chem.*, 2009, 57, 6564.
- (7) M. Ghaedi, M. R. Fathi, A. Shokrollahi, F. Shajarat, *Anal. Lett.*, 2006, 39, 1171.
- (8) G. Giakissikli, M. Miró, A. Anthemidis, *Anal. Chem.*, 2013, 85, 8968.
- (9) Y. K. Yang, K. J. Yook, J. Tae, *J. Am. Chem. Soc.*, 2005, 127, 16760.
- (10) J. Huang, X. Gao, J. Jia, J. K. Kim, Z. G. Li, *Anal. Chem.*, 2014, 86, 3209.
- (11) W. P. Wang, Y. C. Lu, H. Huang, A. J. Wang, J. R. Chen, J. J. Feng, *Biosens. Bioelectron.*, 2015, 64, 517.
- (12) C. N. R. Rao, H. S. S. R. Matte, U. Maitra, *Angew. Chem. Int. Ed.*, 2013, 52, 13162.
- (13) Z. Zeng, Z. Yin, X. Huang, H. Li, Q. He, G. Lu, F. Boey, H. Zhang, *Angew. Chem. Int. Ed.*, 2011, 50, 11093.
- (14) Z. Zeng, T. Sun, J. Zhu, X. Huang, Z. Yin, G. Lu, Z. Fan, Q. Yan, H. Hng, H. H. Zhang,

1
2
3 Angew. Chem. Int. Ed., 2012, 51, 9052.

4
5 (15) V. Nicolosi, M. Chhowalla, M. G. Kanatzidis, M. S. Strano, *Science*, 2013, 340, 1226419.

6
7 (16) C. Tan, H. Zhang, *Chem. Soc. Rev.*, DOI: 10.1039/c4cs00182f.

8
9 (17) H. Li, J. Wu, Z. Yin, H. Zhang, *Acc. Chem. Res.*, 2014, 47, 1067.

10
11 (18) X. Huang, C. Tan, Z. Yin, H. Zhang, *Adv. Mater.*, 2014, 26, 2185.

12
13 (19) R. Ganatra, Q. Zhang, *ACS Nano*, 2014, 8, 4074.

14
15 (20) J. Liu, Z. Zeng, X. Cao, G. Lu, L. H. Wang, Q. L. Fan, W. Huang, H. Zhang, *Small*, 2012,
16
17 8, 3517.

18
19 (21) Z. Yin, H. Li, H. Li, L. Jiang, Y. Shi, Y. Sun, G. Lu, Q. Zhang, X. Chen, H. Zhang, *ACS*
20
21 *Nano*, 2012, 6, 74.

22
23 (22) J. Chen, X. J. Wu, L. Yin, B. Li, X. Hong, Z. Fan, B. Chen, C. Xue, H. Zhang, *Angew.*
24
25 *Chem. Int. Ed.*, 2015, 54, 1210.

26
27 (23) S. Wu, Z. Zeng, Q. He, Z. Wang, S. J. Wang, Y. Du, Z. Yin, X. Sun, W. Chen, H. Zhang,
28
29 *Small*, 2012, 8, 2264.

30
31 (24) N. Wang, F. Wei, Y. Qi, H. X. Li, L. Lu, G. Q. Zhao, Q. Xu, *ACS Appl. Mater. Interf.*,
32
33 2014, 6, 19888.

34
35 (25) L. Wang, Y. L. Li, F. Zhang, L. Lin, S. M. Niu, D. Chenet, X. Zhang, Y. F. Hao, T. F.
36
37 Heinz, J. Hone, Z. L. Wang, *Nature*, 2014, 514, 470.

38
39 (26) M. A. Lukowski, A. S. Daniel, F. Meng, A. Forticaux, L. S. Li, S. Jin, *J. Am. Chem. Soc.*,
40
41 2013, 135, 10274.

42
43 (27) C. B. Ma, X. Qi, B. Chen, S. Bao, Z. Yin, X. J. Wu, Z. Luo, J. Wei, H. L. Zhang, H.
44
45 Zhang, *Nanoscale*, 2014, 6, 5624.

46
47 (28) X. Huang, Z. Zeng, S. Bao, M. Wang, X. Qi, Z. Fan, H. Zhang, *Nat. Commun.*, 2013, 4,
48
49 1444.

50
51 (29) K. Zhang, H. J. Kim, X. Shi, J. T. Lee, J. M. Choi, M. S. Song, J. H. Park, *Inorg. Chem.*,
52
53
54
55
56
57
58
59
60

1
2
3 2013, 52, 9807.

4
5 (30) K. Chang, W. X. Chen, ACS Nano, 2011, 5, 4720.

6
7 (31) X. Cao, Y. Shi, W. Shi, X. Rui, Q. Yan, J. Kong, H. Zhang, Small, 2013, 9, 3433.

8
9 (31) C. F. Zhu, Z. Y. Zeng, H. Li, F. Li, C. H. Fan, H. Zhang, J. Am. Chem. Soc., 2013, 135,
10 5998.

11
12 (32) C. L. Tan, X. Y. Qi, X. Huang, J. Yang, B. Zheng, Z. F. An, R. F. Chen, J. Wei, B. Z.
13 Tang, W. Huang, H. Zhang, Adv. Mater., 2014, 26, 1735.

14
15 (34) C. Zhu, Z. Zeng, H. Li, F. Li, C. Fan, H. Zhang, J. Am. Chem. Soc., 2013, 135, 5998.

16
17 (35) Y. Zhang, B. Zheng, C. Zhu, X. Zhang, C. Tan, H. Li, B. Chen, J. Yang, J. Chen, Y.
18 Huang, L. Wang, H. Zhang, Adv. Mater., 2015, 27, 935.

19
20 (36) T. Palacios, Nat. Nanotechnol., 2011, 6, 464.

21
22 (37) M. Chhowalla, H. S. Shin, G. Eda, L. J. Li, K. P. Loh, H. Zhang, Nat. Chem., 2013, 5,
23 263.

24
25 (38) X. Huang, Z. Y. Zeng, H. Zhang, Chem. Soc. Rev., 2013, 42, 1934.

26
27 (39) H. Terrones, F. Lopez-Urias, M. Terrones, Sci. Rep., 2013, 3, 1549.

28
29 (40) R. Lv, J. A. Robinson, R. E. Schaak, D. Sun, Y. F. Sun, T. E. Mallouk, M. Terrones, Acc.
30 Chem. Res., 2014, doi.org/10.1021/ar5002846.

31
32 (41) J. F. Xie, H. Zhang, S. Li, R. X. Wang, X. Sun, M. Zhou, J. F. Zhou, X. W. Lou, Y. Xie,
33 Adv. Mater., 2013, 25, 5807.

34
35 (42) D. Gopalakrishnan, D. Damien, M. M. Shaijumon, ACS Nano, 2014, 8, 5297.

36
37 (43) L. M. Yang, K. Majumdar, H. Liu, Y. C. Du, H. Wu, M. Hatzistergos, P. Y. Hung, R.
38 Tieckelmann, W. Tsai, C. Hobbs, P. Ye, Nano Lett., 2014, doi.org/10.1021/nl502603d.

39
40 (44) S. McDonnell, R. Addou, C. Buie, R. M. Wallace, C. L. Hinkle, ACS Nano, 2014, 8,
41 2880.

42
43 (45) J. Z. Ou, A. F. Chrimes, Y. C. Wang, S. Y. Tang, M. S. Strano, K. Kalantar-zadeh, Nano
44
45
46
47
48
49
50
51
52
53
54
55
56
57
58
59
60

1
2
3 lett., 2014, 14, 857.

4
5 (46) Y. Wang, J. Z. Ou, S. Balendhran, A. F. Chrimes, M. Mortazavi, D. D. Yao, M. Field, K.
6
7 Field, V. Bansal, J. R. Friend, S. Zhuiykov, N. V. Medhekar, M. S. Strano, K. Kalantar-zadeh,
8
9 ACS nano, 2013, 7, 10083.

10
11 (47) D. H. Hyun, J. H. Dong, S. C. Jong, P. Minsu, S. S. Tae, Small, 2014, 10, 3858.

12
13 (48) R. Freeman, T. Finder, I. Willner, Angew. Chem. Int. Ed., 2009, 48, 7818.

14
15 (49) L. Zhou, Y. H. Lin, Z. Z. Huang, J. S. Ren, X. Q. Qu, Chem. Commun., 2012, 48, 1147.

16
17 (50) B. Paramanik, S. Bhattacharyya, A. Patra, Chem. Eur. J., 2013, 19, 5980.

18
19 (51) S. J. He, B. Song, D. Li, C. F. Zhu, W. P. Qi, Y. Q. Wen, L. H. Wang, S. P. Song, H. P.
20
21 Fang, C. H. Fan, Adv. Funct. Mater., 2010, 20, 453.

22
23 (52) L. Shang, J. Yin, J. Li, L. Jin, S. Dong, Biosens. Bioelectron., 2009, 25, 269.

24
25 (53) N. Y. Fu, Y. Q. Chen, J. Fan, G. M. Wang, S. Y. Lin, Sens. Actuators B Chem., 2014, 203,
26
27 435.

28
29 (54) L. Wang, T. Yao, S. Shi, Y. L. Cao, W. L. Sun, Sci. Rep., 2014, 4, 5320.

30
31 (55) Y. P. Zhu, T. Y. Ma, T. Z. Ren, Z. Y. Yuan, ACS Appl. Mater. Interf., 2014, 6, 16344.

32
33 (56) X. Cui, L. Zhu, J. Wu, Y. Hou, P. Y. Wang, Z. N. Wang, M. Yang, Biosens. Bioelectron.,
34
35 2015, 63, 506.

36
37 (57) H. L. Li, J. F. Zhai, J. Q. Tian, Y. L. Luo, X. P. Sun, Biosens. Bioelectron., 2011, 26,
38
39 4656.

40
41 (58) F. M. Kin, L. Changgu, H. James, S. Jie, F. H. Tony, Phys. Rev. Lett., 2010, 105, 136805.

42
43 (59) X. B. Chen, L. Liu, P. Y. Yu, S. S. Mao, Science, 2011, 311, 746.
44
45
46
47
48
49
50
51
52
53
54
55
56
57
58
59
60